

Elliptic flow (v_2) in pp collisions at energies available at the CERN Large Hadron Collider: A hydrodynamical approach

S. K. Prasad, Victor Roy, S. Chattopadhyay, and A. K. Chaudhuri
Variable Energy Cyclotron Centre, 1/AF Bidhan Nagar, Kolkata 700 064, India
(Dated: October 31, 2018)

At Large Hadron Collider energy, the expected large multiplicities suggest the presence of collective behavior even in pp collisions. A hydrodynamical approach has been applied to estimate the expected elliptic flow measured by the azimuthal asymmetry parameter v_2 in pp collisions at $\sqrt{s} = 14$ TeV. v_2 of π^- is found to be strongly dependent on the parton density profile inside a proton [e.g., surface diffuseness parameter (ξ)]. For $\xi = 0.105$ fm, v_2 is found to be positive and larger compared to that at $\xi = 0.25$ fm. The centrality dependence of v_2 has also been studied.

I. INTRODUCTION

The elliptic flow is found to be one of the most interesting observables at the relativistic heavy-ion collider (RHIC). Large elliptic flow in noncentral Au+Au collisions confirms fluidlike behavior of the produced matter [1]. Elliptic flow measures the momentum anisotropy of the produced particles. In noncentral collisions between two identical nuclei, the reaction zone is spatially asymmetric. The rescattering process among the produced particles (locally isotropic in momentum space) transfers this spatial asymmetry into the momentum space, and the momentum distribution of the produced particles becomes anisotropic. Elliptic flow is an early time phenomenon. It is a sensitive probe to the: (i) degree of thermalization, (ii) equation of state (EOS), and (iii) transport coefficients [2–6].

In pp collisions at RHIC energy, the average multiplicity $\langle n_{ch} \rangle$ is significantly low for any collective effects to be seen, however, detailed studies of various observables e.g., Hanbury-Brown-Twiss parameters [7] and charged particle spectra gave hints that even in pp collisions, collective models (e.g., hydrodynamics) might give a satisfactory explanation for a large part of the data. Applicability of hydrodynamics in a small system such as pp is uncertain. Hydrodynamics requires local thermal equilibration, which can be achieved only if the mean-free path of the constituents is small compared to the size of the system $\lambda \ll R$. In pp collisions, size of the system is not large $\lambda \sim R \sim 1$ fm. However, in Ref. [8], it is argued that, if the medium is isotropized within a time scale τ_i , hydrodynamics may be applicable beyond τ_i . See Ref. [8] and references therein, where the applicability of hydrodynamics in central pp collisions after $\tau_i \sim 0.2$ fm is justified. The scenario of collective expansion of matter created in pp collisions at Large Hadron Collider (LHC) energy is discussed in Ref. [9]. The expectation that hydrodynamics can be applicable in high-energy proton-proton collision is not new, for example, see Ref. [10]. Recently, the possibility to observe a collective expansion signal - in the form of an azimuthal anisotropy of particle production with respect to the reaction plane - caused by multipartonic interactions in proton-proton collisions at the LHC is studied [11]. In

Ref. [11], different values of integrated v_2 are predicted, which range from -3% to 10% depending upon the profile of matter distribution in transverse space of the colliding protons, and it is argued that the study of hadron anisotropy with respect to the reaction plane in pp collisions at LHC energies can provide important information on the proton shape and structure. In Ref. [12], large elliptic flow $v_2 \sim 10$ -20% is predicted in high-multiplicity pp collisions at the LHC if hot-spot-like structures are produced in the initial collisions.

In pp collisions at LHC energies, average multiplicity will increase, and there could be events with multiplicity comparable to the multiplicity in peripheral Au+Au collisions at the RHIC. A picture based on two separate transverse distance scales in pp collisions at higher energies gives an impact-parameter dependence of pp inelastic (INEL) collisions. In the case of central pp collisions, the distribution of hard partons ($x \geq 10^{-2}$) in the two colliding nucleons will overlap, while in large impact-parameter collisions, partons with $x \ll 10^{-2}$ will overlap with significant probability [13]. A trigger on hard dijet production can quantitatively distinguish between a central and a peripheral collision. In this scenario, these high-energy pp collisions can pictorially be represented as AA collisions, and the impact-parameter dependence of initial eccentricity ε_x can be estimated. Significantly large energy density, which generates large multiplicity in pp collisions at the LHC will lead to rescatterings, thereby creating a system where hydrodynamics can be applied and the parameters such as v_2 can be estimated. Here we report the results obtained by applying the hydrodynamic evolution to the system formed in pp collisions at the LHC energy ($\sqrt{s} = 14$ TeV).

The paper is organized in the following way. Section II describes the details of the code (AZYHYDRO) used for the hydrodynamic evolution of the system, and we explain how we incorporated the impact-parameter dependence of the pp INEL cross section. In Sec. III, the results are presented and are discussed. We have explained how the initial energy density is chosen for the hydrodynamic evolution of the system at $\sqrt{s} = 14$ TeV. The p_t spectra, mean p_t , dN/dy , spatial eccentricity, and v_2 with their dependence on impact parameter b or p_t are presented. In Sec. IV, we summarize our results and conclude.

II. THE HYDRODYNAMIC MODEL

We briefly describe the hydrodynamic model used to obtain space-time evolution of fluid formed in pp collisions. Details can be found in Refs. [14, 15]. The equation of motion of a relativistic ideal fluid follows from the local conservation laws of energy and momentum, and other conserved currents (e.g., baryon number),

$$\partial_\mu T^{\mu\nu}(x) = 0 \quad (1)$$

$$\partial_\mu j^\mu(x) = 0. \quad (2)$$

Ideal fluid decompositions of energy-momentum tensor ($T^{\mu\nu}$) and baryon four-current (j^μ) are as follows:

$$T^{\mu\nu}(x) = [e(x) + p(x)]u^\mu(x)u^\nu(x) - g^{\mu\nu}p(x), \quad (3)$$

$$j^\mu(x) = n(x)u^\mu(x), \quad (4)$$

where $e(x)$ is the energy density, $p(x)$ is the pressure, and $n(x)$ is the conserved baryon number density at point $x^\mu = \{t, x, y, z\}$. u^μ is the hydrodynamic four-velocity, $u^\mu = \gamma(1, v_x, v_y, v_z)$ with $\gamma = \frac{1}{\sqrt{(1-v_x^2-v_y^2-v_z^2)}}$. The publicly available AZHYDRO code solves 2+1-dimensional hydrodynamics. At high collision energies, relativistic kinematics and its influence on the particle production process implies longitudinal-boost invariance of the collision fireball near midrapidity [16]. As a result, the longitudinal velocity field scales as $v_z = \frac{z}{t}$, and it is convenient to use a coordinate system spanned by longitudinal proper time $\tau = t\sqrt{1-v_z^2}$ and the space-time rapidity $\eta = \frac{1}{2}\ln[\frac{t+z}{t-z}]$ instead of t and z . Longitudinal-boost invariance is then equivalent to η independence. By assuming the longitudinal-boost invariance, we reduce the number of energy-momentum conservation equations from four to three, viz. two transverse and one time. This will restrict us as we see the effect of rapidity dependence of transverse flow pattern.

The initial thermalization stage lies outside the domain of applicability of hydrodynamical approach and must be replaced by the initial condition for the hydrodynamical evolution. We assume that the fluid is thermalized at the initial time τ_i . We have systematically performed the calculations for three different values of τ_i (0.2, 0.4, and 0.6 fm). At the initial time, transverse velocity of the fluid is zero $v_x(x, y) = v_y(x, y) = 0$. At an impact-parameter b , the initial energy density is assumed to be distributed as

$$\epsilon_i(x, y, \mathbf{b}) = \epsilon_0 N_{coll}(x, y, \mathbf{b}), \quad (5)$$

where $N_{coll}(x, y, \mathbf{b}) \propto T(x + \frac{b}{2}, y)T(x - \frac{b}{2}, y)$ is a Glauber model calculation for the transverse profile of the (partonic) binary collisions at impact parameter \mathbf{b} . The central energy density ϵ_0 does not depend on the impact parameter of the collisions.

For the Glauber model calculation of collision number distribution, we assume a Woods-Saxon profile for the (partonic) density distribution of the colliding protons,

$$\rho(r) = \frac{\rho_0}{1 + e^{(r-R)/\xi}} \quad (6)$$

with $R=1.05$ fm. The calculations are performed at two values of proton diffuseness parameter (i.e., $\xi = 0.105$ fm and $\xi = 0.25$ fm) (see Ref. [11] and references therein). The value of ρ_0 is fixed in such a way that the total INEL cross section in pp collisions at a given energy is reproduced in the Glauber model calculation. The values of ρ_0 , required to produce the INEL cross section are 0.45 and 0.70 at $\sqrt{s} = 0.2$ and 14 TeV, respectively, for $\xi = 0.25$. The total INEL cross sections in pp collisions at $\sqrt{s} = 0.2$ and 14 TeV are taken to be 40 and 80 mb, respectively. The parton-proton thickness function is given by the optical path length:

$$T(x, y) = \int_{-\infty}^{\infty} \rho(x, y, z) dz. \quad (7)$$

Hydrodynamical equations Eq.1, and 2 are closed only with an EOS $p = p(e, p)$. We have used the EOS, which is composed of lattice EOS and hadron resonance gas EOS. Recently Cheng *et.al.* [17] presented high statistics lattice QCD results for the bulk thermodynamic observables (e.g., pressure, energy density, entropy, etc.). We have parametrized the entropy density as

$$\frac{s}{T^3} = \alpha + [\beta + \gamma][1 + \tanh \frac{T - T_c}{\delta T}]. \quad (8)$$

The values of the parameters α, β, γ are chosen in such a way that the lattice simulation of s/T^3 is best fitted [18]. We have taken the crossover temperature $T_c = 196$ MeV. From the parametric form of entropy density, pressure and energy density can be obtained by using the thermodynamic relations:

$$p(T) = \int s(T') dT', \quad (9)$$

$$\epsilon(T) = Ts - p. \quad (10)$$

We complement the lattice EOS [17] by a hadronic resonance gas (HRG) EOS, which comprises all the resonances below the mass 2.5 GeV. The entropy density of complete EOS is obtained as,

$$s = 0.5[1 + \tanh(x)]s_{HRG} + 0.5[1 - \tanh(x)]s_{LATTICE} \quad (11)$$

with $x = \frac{T - T_c}{\delta T}$, $\delta T = 0.1 T_c$. s_{HRG} is the entropy density for HRG, and $s_{LATTICE}$ is the entropy density for lattice.

As the system expands, its volume increases, and the density decreases, as a result, after some time, the mean-free path of the particles becomes larger than the system size, and the concept of local thermalization breaks down. Thus, the hydrodynamic evolution has to be stopped by applying the freeze-out criteria. We assume that freeze

out occurs at a fixed temperature T_F . We have used three different values of T_F (130, 140, and 150 MeV) in our calculation. By using the standard Cooper-Frye formalism [19], we calculate the invariant distribution of particles at the freeze-out hypersurface. In the Cooper-Frye formalism, the invariant distribution is given by the following equation:

$$E \frac{dN_i}{d^3p} = \frac{dN_i}{dy p_T dp_T d\phi} = \frac{g_i}{(2\pi)^3} \int_{\Sigma} f_i(p \cdot u(x), x) p^\mu d^3\sigma_\mu, \quad (12)$$

where $d^3\sigma_\mu$ is the outward normal vector on the freeze-out hypersurface Σ such that $p^\mu f_i d^3\sigma_\mu$ is the local flux of particles with the momentum p through this surface, and the distribution function is

$$f_i(E, x) = \frac{1}{\exp\left[\frac{(E - \mu_i(x))}{T(x)}\right] \pm 1}. \quad (13)$$

By applying Lorentz boost, we will get the value of local flow velocity $u^\mu(x)$ to the global reference frame by the substitution $E \rightarrow p^\mu u_\mu$, where $\mu_i(x)$ and $T(x)$ are the chemical potential of particle species i and the local temperature along hypersurface Σ , respectively. From the invariant distribution, particle multiplicity (dN_{ch}/dy), mean p_T ($\langle p_T \rangle$), elliptic flow (v_2), etc., can easily be computed.

III. RESULTS

A. Estimation of initial energy density in pp collisions at LHC

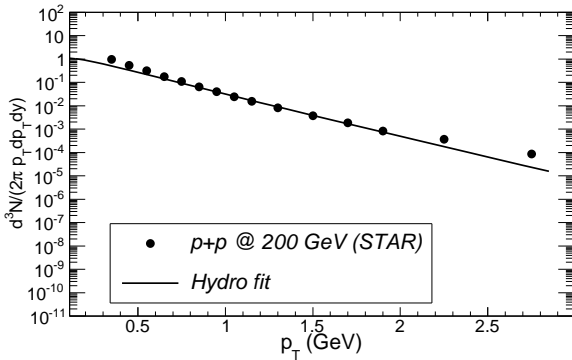


FIG. 1: The filled circles are the RHIC data for the transverse momentum distribution for π^- in pp collisions at $\sqrt{s} = 200$ GeV. The solid line is the hydrodynamical model fit to the data at diffuseness parameter $\xi = 0.25$ fm.

In the absence of experimental guidance in pp collisions at the LHC ($\sqrt{s} = 14$ TeV), it is difficult to fix the initial energy density ϵ_i for hydrodynamical calculations in pp collisions at the LHC. We choose the initial energy density such that the experimentally measured or extrapolated values of $dN_{ch}/d\eta$ in pp collisions at given \sqrt{s} is

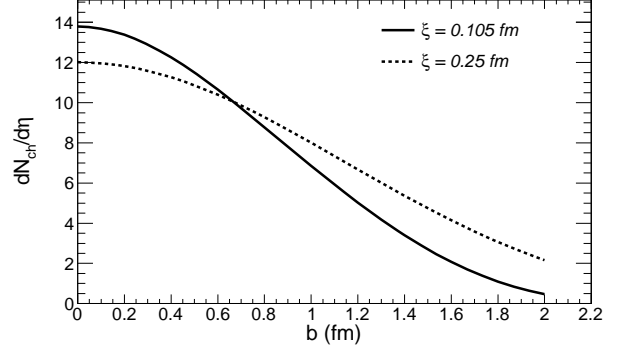


FIG. 2: Variation of dN_{ch}/dy with impact parameter b , for $\sqrt{s} = 14$ TeV for $\xi = 0.25$ fm (dotted line) and $\xi = 0.105$ fm (solid line).

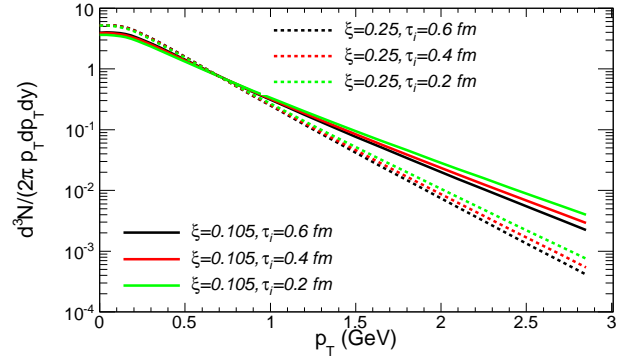


FIG. 3: (Color online) The minimum bias p_T spectra for three initial times ($\tau_i = 0.2, 0.4, 0.6$ fm), with $\xi = 0.25$ fm (dotted lines) and $\xi = 0.105$ fm (solid lines) at $\sqrt{s} = 14$ TeV.

reproduced. We have fitted the experimentally measured p_T spectra of π^- in pp collisions at $\sqrt{s} = 200$ GeV from the STAR experiment at the RHIC, and they are shown in Fig.1. The filled circles are the RHIC data points for the transverse momentum distribution of π^- . The solid line is the hydrodynamical model fit to the data with proton diffuseness parameter $\xi = 0.25$ fm. Note that the pp collisions are measured at minimum bias, without any centrality or impact-parameter dependence. To compare the experimental data with hydrodynamic simulations, we compute the minimum bias spectra as

$$\frac{dN}{dy d^2p_T} = \frac{\int_0^{b_{max}} 2\pi b \frac{dN(b)}{dy d^2p_T} db}{\int_0^{b_{max}} 2\pi b db} \quad (14)$$

where $\frac{dN(b)}{dy d^2p_T}$ is the π^- invariant distribution at an impact parameter b . We have integrated upto $b_{max} = 1.6$ fm, which covers $\sim 90\%$ of the INEL cross section. Generally, one does not apply hydrodynamics in pp collisions. The system size possibly is too small for macroscopic concepts to be valid. However, in Ref. [10], there are some discussions on applications of hydrodynamical calcula-

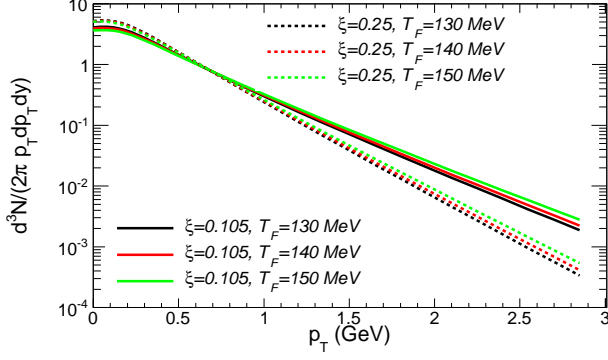


FIG. 4: (Color online) The minimum bias p_T spectra for three freeze-out temperatures ($T_F = 130, 140, 150$ MeV) with $\xi = 0.25$ fm (dotted lines) and $\xi = 0.105$ fm (solid lines) at $\sqrt{s} = 14$ TeV.

tions to such systems. We observe that the p_T spectra as measured by the STAR Collaboration at the RHIC ($\sqrt{s} = 200$ GeV) for pp collisions is reasonably well explained in the hydrodynamic model. In the low p_T region $p_T < 0.5$ GeV/c, the simulation underestimates the data because a large fraction of low p_T pions are probably coming from various resonance decays, which are not considered in the simulation. Agreement with data in the low p_T region will improve if resonance contributions are accounted for. Hydrodynamical simulation also underestimates the data at high $p_T > 2$ GeV/c, which indicates departure from ideal hydrodynamics because of dissipative effects. Also, at large p_T , sources other than hydrodynamics contribute to particle production.

Charged-particle pseudorapidity distribution in the central rapidity region in p+p and p+ \bar{p} interactions is expected to have a power-law dependence on center-of-mass energy [20]. Therefore, we use the relation,

$$\left. \frac{dN_{ch}}{dy} \right|_{LHC} = a \times (\sqrt{s}_{LHC})^b, \quad (15)$$

where a and b are the parameters whose values are obtained as $a = 0.7166$ and $b = 0.2171$ by fitting the \sqrt{s} dependence of INEL charged-particle pseudorapidity density in the central rapidity region in p+p and p+ \bar{p} interactions [20]. The extrapolated minimum bias charged particles pseudorapidity density at $y = 0$ at the LHC ($\sqrt{s} = 14$ TeV) is determined to be 5.69. For performing simulations at the LHC, the initial energy density is fixed accordingly. The energy density required to reproduce the extrapolated $dN_{ch}/d\eta$ is different for different values of initial time (τ_i) and freeze-out temperature (T_F).

B. Mean multiplicity (dN/dy), mean p_t ($\langle p_t \rangle$) and p_t spectra

The parameters that are used in this calculation for pp collisions need to be varied as these parameters can

be fixed only after detailed experimental investigations. Therefore, we perform our calculations for three different values of freeze-out temperature ($T_F = 130, 140$, and 150 MeV) and three different values of initial time ($\tau_i = 0.2, 0.4$, and 0.6 fm) with two values of diffuseness parameter ($\xi = 0.25$ fm and $\xi = 0.105$ fm).

The initial energy density (ϵ_i), the minimum bias average multiplicity ($\frac{dN_{ch}}{dy}$) at $y = 0$, the mean p_T , and the p_T integrated v_2 in pp collisions at LHC energy ($\sqrt{s} = 14$ TeV), are calculated and are summarized in Tables I and II for various initial conditions at two values of diffuseness parameters.

TABLE I: The minimum bias multiplicity dN_{ch}/dy , the mean p_T and the p_T integrated v_2 for various freeze-out temperatures for both diffuseness parameters at a fixed τ_i .

τ_i (fm)	ξ (fm)	T_F (MeV)	ϵ_i (GeV/ fm^3)	dN_{ch}/dy	$\langle p_T \rangle$ (GeV/c)	v_2 (%)
0.6	0.25	130	20.7	5.68	0.56	0.34
0.6	0.25	140	26.2	5.68	0.57	0.37
0.6	0.25	150	35.0	5.68	0.59	0.40
0.6	0.105	130	31.4	5.69	0.68	1.38
0.6	0.105	140	40.0	5.69	0.70	1.38
0.6	0.105	150	53.8	5.69	0.73	1.40

TABLE II: The minimum bias multiplicity dN_{ch}/dy , the mean p_T and the p_T integrated v_2 for various initial times for both diffuseness parameters at a fixed T_F .

T_F (MeV)	ξ (fm)	τ_i (fm)	ϵ_i (GeV/ fm^3)	dN_{ch}/dy	$\langle p_T \rangle$ (GeV/c)	v_2 (%)
140	0.25	0.2	99.7	5.69	0.60	0.34
140	0.25	0.4	42.5	5.68	0.59	0.35
140	0.25	0.6	26.2	5.68	0.57	0.37
140	0.105	0.2	160.7	5.69	0.76	1.32
140	0.105	0.4	66.5	5.69	0.72	1.30
140	0.105	0.6	40.0	5.69	0.70	1.38

At a fixed initial time ($\tau_i = 0.6$ fm), when the freeze-out temperature is increased from 130 to 150 MeV, the mean p_T is found to increase by 5.3% and 7.3% whereas the p_T integrated v_2 is found to increase by 17.6% and 1.4% for $\xi = 0.25$ and 0.105 fm, respectively. At a fixed freeze-out temperature ($T_F = 140$ MeV), when the initial time is increased from 0.2 to 0.6 fm, the mean p_T is found to decrease by 5.0% and 7.8%, whereas the p_T integrated v_2 is found to increase by 8.8% and 4.5% for $\xi = 0.25$ and 0.105 fm, respectively. However, the mean p_T is however, found to be consistently higher for the case with $\xi = 0.105$ fm as compared to the case with $\xi = 0.25$ fm. The reason is understood. For the sharp proton density distribution ($\xi = 0.105$ fm), fluid is initialized with higher energy density as compared to that when the surface is more diffused ($\xi = 0.25$ fm). Increased transverse pressure in the fluid then leads to increased mean p_T .

In Fig.2, we have shown the impact-parameter dependence of dN_{ch}/dy at $y = 0$ for both values of diffuseness parameter $\xi = 0.105$ fm and $\xi = 0.25$ fm. As expected,

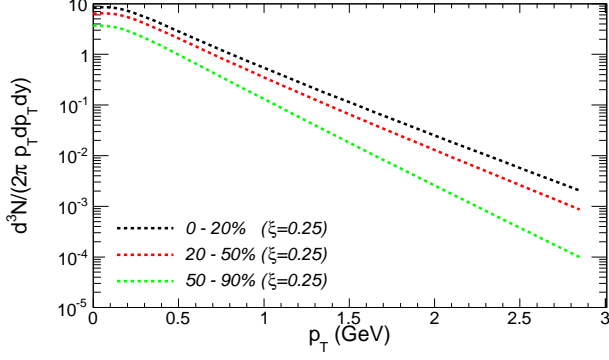


FIG. 5: (Color online) The p_T spectra for three different centralities with $\xi = 0.25$ fm.

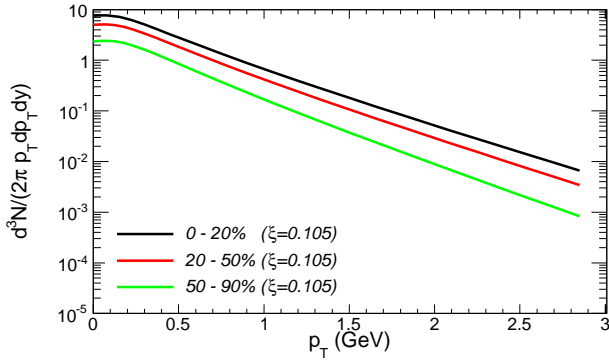


FIG. 6: (Color online) The p_T spectra for three different centralities with $\xi = 0.105$ fm.

charged-particle rapidity density decreases with increasing impact parameters for both ξ . This indicates that higher multiplicity events in pp collisions are obtained at low-impact parameters, and a centrality trigger based on multiplicity might select these interesting events. The rapidity density of charged particles at mid rapidity for $b = 0$ is 13.79 for $\xi = 0.105$ fm and 12.01 for $\xi = 0.25$ fm. The impact-parameter dependence of rapidity density of a charged particle for two diffuseness parameters shows an interesting feature, that for $\xi = 0.105$ fm, the rapidity density of charged particles reduces faster as their configuration is close to the hard sphere; and above some impact parameter, the overlap region reduces faster. The result is according to our expectation. In peripheral collisions, the overlap region is comparatively large when the surface is more diffused. The impact parameter dependence of rapidity density of charged particles can be predicted to provide size information on the diffuseness parameter of the colliding protons.

The minimum bias p_T spectra of charged particles for different values of initial times and freeze-out temperature are shown in Figs.3 and 4, respectively. Minimum bias p_T spectra are obtained by integrating up to $b_{max} = 1.6$ fm, which, as previously indicated, covers $\sim 90\%$

of INEL cross section. It is observed that the p_T spectra are not affected much because of the change in freeze-out temperature and in initial time for a particular diffuseness parameter. However, the spectra are different for different diffuseness parameters. Note that, whenever there is a change in either T_F at fixed τ_i or in τ_i at fixed T_F , the initial energy density (ϵ_i) is adjusted accordingly so that the average multiplicity (dN_{ch}/dy) is always fixed.

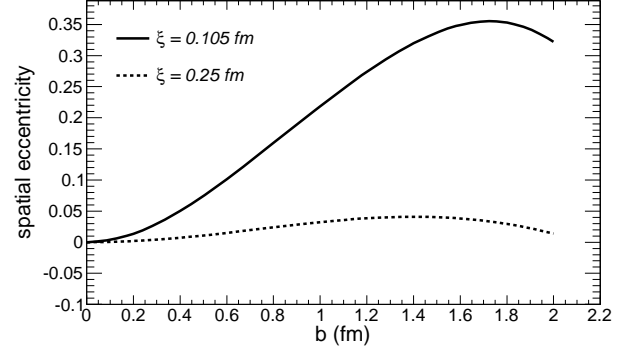


FIG. 7: Initial spatial eccentricity, ε_x as a function of impact parameter for pp collisions at $\sqrt{s} = 14$ TeV for $\xi = 0.25$ fm (dotted line) and $\xi = 0.105$ fm (solid line).

As discussed earlier, the pseudorapidity density of the charged particle is 13.79 and 12.01 for $\xi = 0.105$ fm and $\xi = 0.25$ fm, respectively, at $b = 0$. This suggests that one can possibly determine two to three centralities experimentally on the basis of multiplicity. Therefore, we have studied the centrality (or impact parameter) dependence of p_T spectra, v_2 etc. for three centralities viz. 0 to 20%, 20 to 50% and 50 to 90%. The centrality dependence of p_T spectra for three centralities is shown in Figs.5 and 6 for $\xi = 0.25$ fm and $\xi = 0.105$ fm, respectively. As indicated previously, we have neglected the resonance contribution. Resonance mainly contributes at the low p_T region. Centrality dependence of p_T spectra is qualitatively similar to that obtained in Au+Au collisions at the RHIC at both ξ . As the collisions become more and more peripheral, the slope of the spectra gets steeper, which indicates reduced source temperature. The result is consistent with our expectation. Although the spectra looks similar for both ξ , they differ in details (e.g., slope, total yield, etc.).

C. Elliptic flow (v_2)

The particle azimuthal distribution can be constructed from different quantities such as transverse momentum, multiplicity, or transverse energy in relatively narrow (pseudo)-rapidity windows [21]. For the non zero impact parameter, the azimuthal distribution of the particles in the reaction plane is not symmetric (anisotropic) in ϕ . We can decompose the distribution in terms of Fourier

expansion as

$$E \frac{d^3 N}{d^3 p} = \frac{d^2 N}{2\pi p_t dp_t dy} \times \left\{ \sum (1 + 2v_n \cos(n\phi')) \right\}, \quad (16)$$

where ϕ' is the angle of azimuth of the outgoing particle with respect to the reaction plane. The coefficient of the second term in the Fourier expansion is known as the elliptic flow v_2 . The nonzero v_2 describes the eccentricity of an ellipselike distribution. The origin of the measured anisotropy could be different: hydrodynamical flow, shadowing effect, both, etc. What they have in common is some collective behavior in the evolution of the multiparticle production process [21].

The initial spatial eccentricity of the reaction zone in the transverse plane changes with a change in the impact parameter. The v_2 is sensitive to this change in spatial eccentricity and, consequently, to the change in the impact parameter. Initial spatial eccentricity ε_x is defined as

$$\varepsilon_x(b) = \frac{\langle y^2 - x^2 \rangle}{\langle y^2 + x^2 \rangle}, \quad (17)$$

where the angular brackets denote energy density weighted averages at the initial time τ_i . In Fig.7, initial eccentricity ε_x , for the two values of diffuseness parameter $\xi = 0.25$ fm and $\xi = 0.105$ fm, are shown as a function of the impact parameter. For diffused protons ($\xi = 0.25$ fm), the spatial eccentricity does not grow significantly. However, for the small diffuseness parameter, $\xi = 0.105$ fm, the spatial eccentricity ε_x increases with the impact parameter and reaches a maximum at midcentral collisions. The behavior is similar to that of Au+Au collisions.

The effect of varying initial conditions (τ_i and T_F) on minimum bias differential elliptic flow ($v_2(p_T)$) is studied, and the results are depicted in Figs. 8 and 9. In Fig. 8, we have plotted the minimum bias differential elliptic flow $v_2(p_T)$ for three values of initial time ($\tau_i = 0.2, 0.4, 0.6$ fm) for both ξ . In Fig. 9, we have plotted the minimum bias differential elliptic flow $v_2(p_T)$ for three values of freeze-out temperature ($T_F = 130, 140, 150$ MeV) for both ξ .

The minimum bias differential elliptic flow [$v_2(p_T)$], is found to be positive for both ξ . The change in $v_2(p_T)$ caused by the change in initial conditions (τ_i or T_F) is negligible. However, $v_2(p_T)$ is found to be very large (reaches up to 24% at $p_T = 3$ GeV/c) for the case with $\xi = 0.105$ fm, whereas for $\xi = 0.25$ fm, it reaches a maximum value up to 6% (at $p_T = 3$ GeV/c).

We have also studied the centrality dependence of p_T integrated v_2 and differential elliptic flow $v_2(p_T)$ for both ξ , for $\tau_i = 0.6$ fm and $T_F = 140$ MeV. The $v_2(p_T)$ for three different centralities is shown in Fig. 10. The differential elliptic flow $v_2(p_T)$ is found to increase when we go toward mid peripheral, which reaches a maximum upto 33% (at $p_T = 3$ GeV/c) for $\xi = 0.105$ fm whereas it reaches a maximum value of 7% for $\xi = 0.25$ fm. The

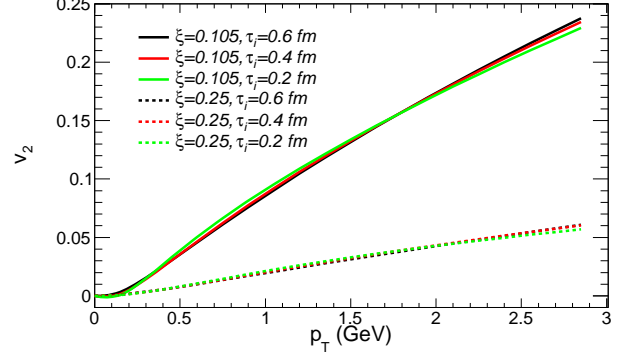


FIG. 8: (Color online) The minimum bias differential elliptic flow $v_2(p_T)$ for three initial times ($\tau_i = 0.2, 0.4, 0.6$ fm) for $\xi = 0.25$ fm (dotted lines) and $\xi = 0.105$ fm (solid lines).

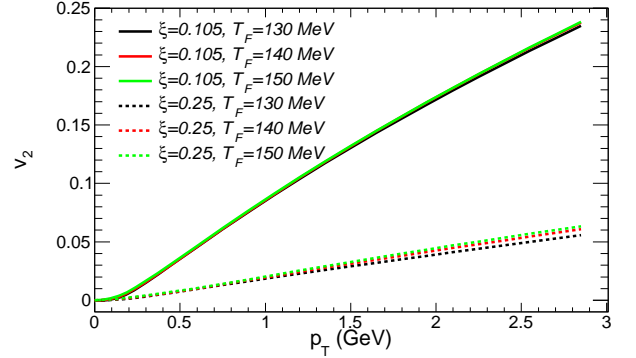


FIG. 9: (Color online) The minimum bias differential elliptic flow $v_2(p_T)$ for three freeze-out temperatures ($T_F = 130, 140, 150$ MeV) for $\xi = 0.25$ fm (dotted lines) and $\xi = 0.105$ fm (solid lines).

centrality dependence of $v_2(p_T)$ is similar for both ξ apart from the differences in their respective values.

The dependence of mean p_T , integrated v_2 , and dN_{ch}/dy with changing the centrality is summarized in Tables III and IV for $\xi = 0.25$ fm and $\xi = 0.105$ fm, respectively.

TABLE III: The minimum bias multiplicity dN_{ch}/dy , the mean p_T , and the p_T integrated v_2 for three different centralities at fixed τ_i (0.6 fm), T_F (140 MeV) and ξ (0.25 fm).

centrality	dN_{ch}/dy	$\langle p_T \rangle$ (GeV/c)	$v_2(\%)$
0-20%	10.78	0.64	0.13
20-50%	7.55	0.60	0.34
50-90%	3.45	0.53	0.29

We observe that the p_T integrated v_2 shows centrality dependence as expected in a hydrodynamic model (i.e., increases when we go from central to midperipheral), however, the value of p_T integrated v_2 is very small. For midcentral collisions, it reaches up to 1.34% and 0.34%

TABLE IV: The minimum bias multiplicity dN_{ch}/dy , the mean p_T , and the p_T integrated v_2 for three different centralities at fixed τ_i (0.6 fm), T_F (140 MeV) and ξ (.105 fm).

centrality	dN_{ch}/dy	$\langle p_T \rangle$ (GeV/c)	v_2 (%)
0-20%	11.74	0.74	0.66
20-50%	7.47	0.71	1.34
50-90%	3.26	0.66	1.23

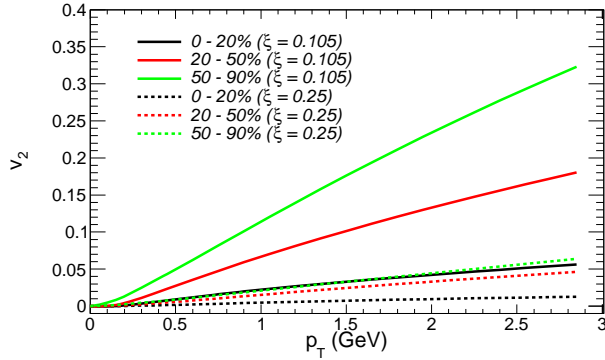


FIG. 10: (Color online) The differential elliptic flow $v_2(p_T)$ for three different centralities for $\xi = 0.25$ fm (dotted line) and $\xi = 0.105$ fm (solid line).

for $\xi = 0.105$ fm and $\xi = 0.25$ fm, respectively.

IV. SUMMARY AND CONCLUSION

To summarize, we have presented a hydrodynamical model study for pp collisions at LHC ($\sqrt{s} = 14$ TeV) en-

ergy. The initial energy density for the hydrodynamic calculation is obtained by requiring a condition that the extrapolated rapidity density of charged particles should be reproduced in the model. After studying the basic properties of particle production (e.g., spectra, dN/dy , $\langle p_T \rangle$, and their centrality dependence), we have extracted v_2 and its dependence on p_t and centralities. As the initial spatial eccentricity depends strongly on the shape of partonic density inside the proton, we have studied two cases of surface diffuseness parameters ξ in Woods-Saxon profile. We have studied the effect of changing initial time τ_i and freeze-out temperature T_F on elliptic flow. It is found that the effect is negligible. The minimum bias differential elliptic flow $v_2(p_T)$ is found to be very large and reaches up to 24% for the case with diffuseness parameter, $\xi = 0.105$ fm. When the diffuseness parameter is 0.25 fm, the minimum bias differential elliptic flow is found to reach up to 6%. At LHC energy, the energy density and particle multiplicity are expected to be substantially large, which suggests the creation of a system that shows collective properties. First results from the LHC [22, 23] have already shown charged multiplicity at the midrapidity region going up to 60. Therefore, we suggest to measure v_2 and its centrality dependence in pp collisions at the LHC. The centrality dependence can be studied by selecting events with different multiplicity bins. The estimation of v_2 at LHC energy might be affected by the presence of nonflow effects (e.g. jets), but methods based on a scalar product, a cumulant or a standard event plane with a large η -gap can be applied. The centrality dependence of v_2 can be used to obtain the surface diffuseness parameter of protons in pp collisions.

-
- [1] K. H. Ackermann *et al.*, [STAR Collaboration] Phys. Rev. Lett **86**, 402 (2001);
C. Adler *et al.*, [STAR Collaboration] Phys. Rev. Lett **87**, 182301 (2001);
S. S. Adler *et al.*, [PHENIX Collaboration] Phys. Rev. Lett **91**, 182301 (2003).
 - [2] J. -Y. Ollitrault, Phys. Rev. D **46**, 229 (1992).
 - [3] J. -Y. Ollitrault, Nucl. Phys. A **638**, 195c (1998).
 - [4] S. Voloshin and Y. Zhang, Z. Phys. C **70**, 665 (1996).
 - [5] P. F. Kolb, U. W. Heinz, P. Huovinen, K. J. Eskola and K. Tuominen, Nucl. Phys. A **696**, 197 (2001).
 - [6] T. Hirano and Y. Nara, Nucl. Phys. A **743**, 305 (2004).
 - [7] Z. Chajecski and M. Lisa, Nucl. Phys. A **830**, 199C (2009).
 - [8] A. K. Chaudhuri, Phys. Lett. B **692**, 15 (2010).
 - [9] Piotr Bozek, Acta Phys. Pol. B **41**, 837 (2010)
 - [10] H. von Gersdorff, Larry McLerran, M. Kataja, P. V. Ruuskanen, Phys. Rev. D **34**, 794 (1986).
 - [11] D. d'Enterria *et al.*, Eur. Phys. J. C **66**, 173 (2010).
 - [12] J. Casalderrey-Solana and U. A. Wiedmann, Phys. Rev. Lett. **104**, 102301 (2010).
 - [13] L. Frankfurt, M. Strikman, and C. Weiss, Phys. Rev. D **69**, 114010 (2004).
 - [14] P. F. Kolb, J. Sollfrank and U. W. Heinz, Phys. Rev. C **62**, 054909 (2000).
 - [15] P. F. Kolb and U. W. Heinz, arXiv:nucl-th/**0305084**.
 - [16] J. D. Bjorken, Phys. Rev. D **27**, 140-151 (1983).
 - [17] M. Cheng *et al.*, Phys. Rev. D **77**, 014511 (2008).
 - [18] A. K. Chaudhuri, Phys. Lett. B **681**, 418 (2009).
 - [19] F. Cooper, G. Frye and E. Schonberg, Phys. Rev. D **11**, 192 (1975).
 - [20] ALICE Collaboration, Eur. Phys. J. C **65** 111 (2010).
 - [21] S. Voloshin, Y. Zhang, Z. Phys. C **70**, 665-672 (1996).
 - [22] ALICE Collaboration, Eur. Phys. J. C **68** 89 (2010).
 - [23] ALICE Collaboration, Eur. Phys. J. C **68** 345 (2010).